

Broadband parametric processes in $\chi^{(2)}$ nonlinear photonic crystals

Matteo Conforti,^{1,*} Fabio Baronio,² Martin Levenius,³ and Katia Gallo³

¹PhLAM/IRCICA, CNRS-Université Lille 1, UMR 8523/USR 3380, F-59655 Villeneuve d'Ascq, France

²Dipartimento di Ingegneria dell'Informazione, Università di Brescia, Via Branze 38, 25123 Brescia, Italy

³Department of Applied Physics, KTH - Royal Institute of Technology, Roslagstullsbacken 21, 10691 Stockholm, Sweden

*Corresponding author: matteo.conforti@univ-lille1.fr

Compiled May 1, 2014

We develop a general model, based on a (2+1)D unidirectional pulse propagation equation, for describing broadband noncollinear parametric interactions in two-dimensional quadratic lattices. We apply it to the analysis of twin-beam optical parametric generation in hexagonally poled LiTaO₃, gaining further insights into experimental observations. © 2014 Optical Society of America

OCIS codes: 190.4410, 190.4360

Introduction. Broadband parametric down-conversion in quadratic $\chi^{(2)}$ quasi phase-matched (QPM) media is crucial for a wide gamut of applications, ranging from quantum optics [1], to high-energy physics [2], sensing [3], and ultrafast spectroscopy [4].

Nowadays, advances in QPM engineering [5] enable purely nonlinear photonic crystals based on two-dimensional (2D) modulations of the $\chi^{(2)}$ nonlinearity [6], affording new degrees of freedom in tailoring the spectral and angular response of parametric devices. Parametric frequency up-conversion in 2D lattices has been extensively investigated in past years [5–7]. **Coupled-mode equations (CME) approaches in frequency domain were shown to accurately model narrowband frequency up-conversion processes [8, 9].** More recently, experiments have addressed also frequency down-conversion, demonstrating enhanced efficiency and tunability of the spectral and angular responses in twin-beam optical parametric generation (TB-OPG) [10, 11]. Key features of the latter can be explained through an intuitive QPM model implying the coherent cross-seeding of concurrent OPG resonances of the lattice via a shared signal (or idler) mode [10]. Simple QPM models, based on standard CME approaches [12], **and also more sophisticated approaches based on Green's function, [8] cannot account** for the extremely rich spectral and angular response observed in the experiments [11], arising from the interplay of multiple concurrent interactions supported by 2D nonlinear lattices, **which give rise to much larger tolerances on wavelength and angular tuning [11, 12].**

In this letter we develop a mathematical model capable of faithfully rendering the complex interaction dynamics arising in the presence of broadband signals and multistep processes in 2D $\chi^{(2)}$ lattices, overcoming the limitations of conventional CME approaches. The model is based on a generalization of the quadratic nonlinear envelope equation, which was recently introduced to describe broadband processes in 1D QPM media [13–18]. To further assess the capabilities of the proposed model,

we apply it to the analysis of infrared TB-OPG in hexagonally poled LiTaO₃ crystals, demonstrating its effectiveness in faithfully reproducing complex details of the angular-spectral response seen in the experiments.

The model. The propagation of a broadband optical pulse in a (2+1) D quadratic medium is ruled by the wave equation for the linearly polarized electric field $E = E(z, x, t)$ [(z, x) and t being the spatial and temporal coordinates, respectively]:

$$\frac{\partial^2 E}{\partial z^2} + \frac{\partial^2 E}{\partial x^2} - \frac{1}{c^2} \frac{\partial^2}{\partial t^2} \int E(t') \varepsilon(t-t') dt' = \frac{1}{\varepsilon_0 c^2} \frac{\partial^2 P_{NL}}{\partial t^2} \quad (1)$$

where $P_{NL} = \varepsilon_0 \chi^{(2)} G(x, z) E^2$ is the second order nonlinear polarization (assumed instantaneous) and $G(x, z)$ describes the modulation of the nonlinear susceptibility. Defining the Fourier transform as $\mathcal{F}[E] = \hat{E}(z, k_x, \omega) = \int E(z, t, x) e^{ik_x x - i\omega t} dx dt$, Eq. (1) can be written in Fourier space as:

$$\frac{\partial^2 \hat{E}}{\partial z^2} + [k^2(\omega) - k_x^2] \hat{E} = -\frac{\omega^2}{\varepsilon_0 c^2} \hat{P}_{NL} \quad (2)$$

where $k^2(\omega) = \varepsilon(\omega) \omega^2 / c^2$. The longitudinal wavenumber can be calculated as $k_z(\omega, k_x) = \sqrt{k^2(\omega) - k_x^2}$. Following the approach outlined in [17, 19], if backward propagating waves can be neglected, a unidirectional pulse propagation equation (UPPE) can be derived:

$$\frac{\partial \hat{E}}{\partial z} + ik_z(\omega, k_x) \hat{E} = -i \frac{\omega^2 \chi^{(2)}}{2k_z(\omega, k_x) c^2} \mathcal{F}[G(x, z) E^2] \quad (3)$$

Equation (3) retains its validity for arbitrarily wide pulse bandwidths, and the computational effort needed to solve it is of the order of magnitude of that needed for solving the standard three-wave equations [20].

Numerical simulations. To test the suitability of the above model (3), we applied it to the study of infrared TB-OPG in hexagonally poled LiTaO₃ crystals, for which experimental results [10, 11] are available for a direct comparison with theoretical predictions.

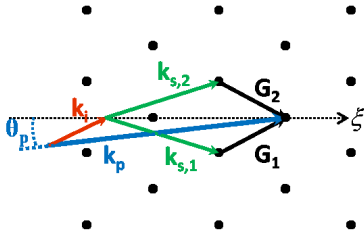


Fig. 1. Sketch of the interaction geometry for TB-OPG with a shared idler, excited by a pump propagating at an angle θ_p to the symmetry axis ξ of the lattice (shown here in reciprocal space). \mathbf{G}_1 and \mathbf{G}_2 are the base lattice vectors used for QPM, k_p , k_i , $k_{s,1}$, are $k_{s,2}$ are the wavevectors of the pump, shared idler and twin-beam signals, respectively.

The interaction geometry is sketched in Fig. 1, where k_p is the wavevector of the OPG pump, propagating at an angle θ_p , close to the grating symmetry axis ξ . The TB-OPG process is sustained by two base reciprocal lattice vectors (RLVs), designated hereafter as \mathbf{G}_1 and \mathbf{G}_2 , which simultaneously quasi phase-match two distinct OPG processes excited by the same pump. Fig. 1 illustrates TB-OPG with specific reference to the case where the two OPG processes share a common idler mode (k_i), producing two frequency-degenerate signal beams ($k_{s,1}$ and $k_{s,2}$).

For a given pump wavelength and propagation angle, the nonlinear resonances for OPG in the lattice are determined by the conservation laws of energy ω and momentum \mathbf{k} of the interacting beams ($p, s, i =$ pump, signal, and idler, respectively, and $m = 1, 2$, corresponding to \mathbf{G}_1 or \mathbf{G}_2):

$$\omega_p = \omega_s + \omega_i, \quad \mathbf{k}_p - \mathbf{G}_m = \mathbf{k}_{s,m} + \mathbf{k}_{i,m} \quad (4)$$

Each RLV (\mathbf{G}_1 or \mathbf{G}_2) can in principle support a continuous set of possible signal-idler pairs of different wavelengths and propagation directions, labelled accordingly with the index 1 or 2. Among such solutions, we are interested in those which can sustain twin-beam OPG, i.e., enable the coherent coupling of two resonances through a shared beam. The shared beam can either be the signal or the idler [11]. We shall refer to these two cases as shared-signal OPG (SS-OPG) and shared-idler OPG (SI-OPG), respectively. In either case, two OPG resonances, coupled by the shared beam, feed each other and produce a twin-beam output at the conjugate wavelength, i.e., degenerate in frequency but non-degenerate in angle.

Simulations of the infrared signal and idler outputs, based on Eq. (3), for OPG in a hexagonal NPC with a period $\Lambda = 22.8\mu\text{m}$, pumped by gaussian pulses at $\lambda_p = 806\text{nm}$, of duration $T_p = 1\text{ps}$, beam waist $W_p = 0.5\text{mm}$ and peak intensity $I_p = 19\text{GW}/\text{cm}^2$, are shown in Fig.2 and 3. Fig. 2 shows the simulated TB-OPG response for the symmetric case ($\theta_p=0$). Normalised output powers for the signal (Fig. 2a) and idler (Fig. 2b) are plot-

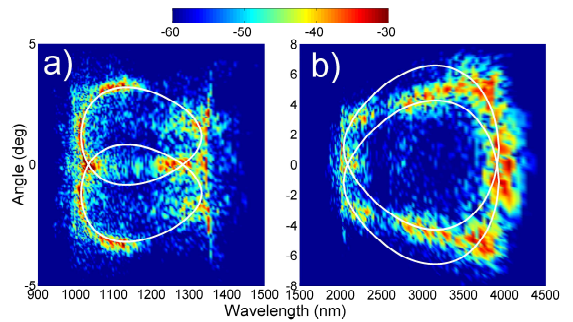


Fig. 2. Spatio-temporal output spectra (dB) obtained from the numerical solution of Eq. (3). Signal (a) and idler (b) generated by a gaussian pump ($\lambda_p = 806\text{nm}$, $T_p = 1\text{ps}$, $W_p = 0.5\text{mm}$, $I_p = 19\text{GW}/\text{cm}^2$) propagating at an angle $\theta_p = 0^\circ$. The white lines are predictions of OPG signals according to Eq. (4)

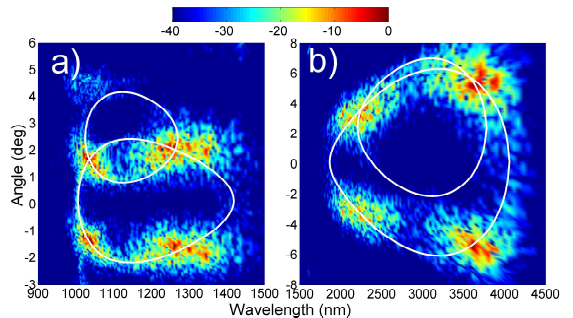


Fig. 3. Same as Fig. 2 for $\theta_p = 0.6^\circ$

ted as a function of wavelength (λ) and angular position (θ) and overlaid with QPM predictions based on Eq. 4 (white lines). In agreement with the intuitive QPM picture, the broadband (2+1)D model highlights enhancements in the overall OPG efficiency whenever a signal (or idler) is shared between the two OPG processes in the lattice (i.e. crossing points of the QPM curves in the OPG maps). Accordingly, in the signal spectra of Fig. 2a enhancements of the on-axis ($\theta=0$) response at 1036 and 1283 nm are ascribed to SS-OPG, while those for off-axis positions at $\lambda_s = 1015$ and 1313 nm (for 806nm pump) to SI-OPG (corresponding to the QPM crossing points at $\theta_i=0$ and $\lambda_i = 3918$ and 2086 nm in Fig. 2b).

As illustrated by the OPG maps of Fig. 2, in contrast to standard QPM approaches, the model (3) affords rigorous and quantitative estimations of the conversion efficiencies and of their distributions for a continuous range of output angles and wavelengths, with a broader spectral coverage, which is particularly relevant for the case of OPG in nonlinear photonic crystals. Besides confirming twin-beam OPG predictions in the framework of shared signal (or idler) OPG, the simulations of Fig.2 highlight also additional effects, such as contributions from non-shared OPG processes at the turning points of the QPM curves (i.e. $\theta_s = \pm 1.2^\circ$, for $\lambda_s = 1010$ and 1350 nm), intuitively justified by the

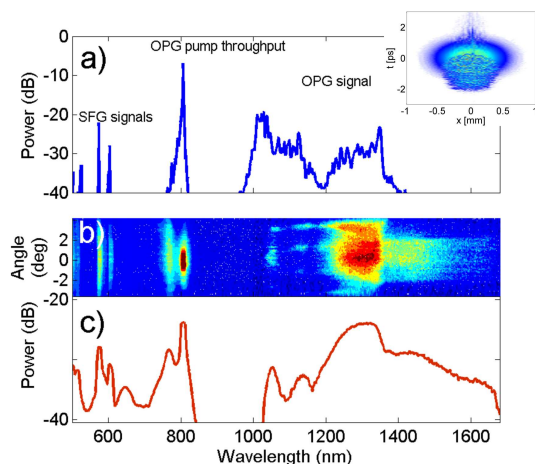


Fig. 4. Output spectra in the symmetric case ($\theta_p = 0^\circ$), corresponding to simulations of Fig. 2. (a) angle-averaged spectra obtained from the model of Eq. (3), (b) experimentally recorded spectral-angular response as a function of output wavelength (λ) and external angle measured with respect to the pump ($\theta - \theta_p$), (c) angle-averaged spectra measured in the range 500-1600nm. **The ≈ 1030 nm OPG peak in (c) is attenuated by the dichroic filter. Inset in (a) shows numerical spatio-temporal output field.**

fact that at these points signal and idler waves are generated collinearly and hence benefit improved spatial overlaps. As a further example of the modelling capabilities of Eq. (3), Fig. 3 shows simulation results for asymmetric TB-OPG with $\theta_p = 0.6^\circ$. OPG signal and idler maps (Fig. 3a and 3b, respectively) clearly illustrate how breaking the symmetry of the TB-OPG interactions by off-axis excitation results in more localised spectral and angular responses, consistently with experimental observations [10]. The maxima of the signal output now clearly stand out from the non-shared OPG background (white lines). The peaks in the signal output located at ($\lambda_s=1037\text{nm}$, $\theta_s = 1.7^\circ$) and ($\lambda_s=1262\text{nm}$, $\theta_s = 2.0^\circ$) arise from SS-OPG, while neighboring peaks at 1255 nm ($\lambda_i = 2254\text{nm}$, $\theta_i=3.6^\circ$) and 1041 nm ($\lambda_i = 3573$ nm, $\theta_i=5.8^\circ$) are due to SI-OPG. Even if the off-axis OPG responses of Fig. 3 exhibit much narrower spectral and angular bandwidths than in the symmetric case (Fig.2), CME approaches are not appropriate for this case either, since each of the OPG maxima is actually stemming from the interplay of at least two OPG resonances (due to the spectral proximity of the SS and SI-OPG working points listed above). On the other hand, such an interplay is likely to be responsible for the broadening and the fine structure in the signal and idler peaks apparent in Fig. 3. Predictions of the full angular and spectral response of NPC lattices provide valuable tools for device design, but also for useful guidelines for the analysis and interpretation of experimental results [11]. This is illustrated through Figs. 4 and 5, where simula-

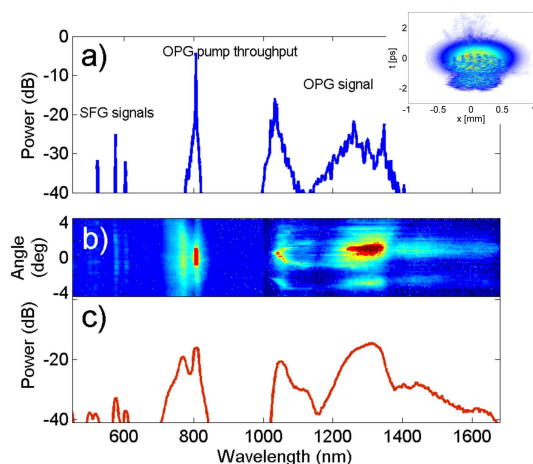


Fig. 5. Same as Fig. 4, for the asymmetric case $\theta_p = 0.6^\circ$, corresponding to the simulations in Fig. 3

tions based on the model of Eq. (3) are compared with experimental findings.

Experiments. Spectral and angular mappings of TB-OPG were obtained from hexagonally poled MgO-doped nearly stoichiometric LiTaO₃ substrates with a 2D period $\Lambda = 22.8\mu\text{m}$ under the experimental conditions detailed in Ref. [11], by using 1 – 1.5ps pump pulses at 1kHz, tunable around 800nm, with peak intensities in the range of 6 – 20GW/cm². Experimental maps of the OPG response for wavelengths between 350 and 1750 nm and angles $-4^\circ \leq \theta \leq 4^\circ$, at different pump incidence angles θ_p between 0° and 1.3° , were retrieved with a Fourier-plane imaging system at the crystal output [11]. Fig. 4 and 5 compare theoretical predictions (a) with measurements (b-c) for the cases of symmetric and asymmetric TB-OPG considered in Fig. 2 and 3, respectively. The data are plotted in the visible to infrared range, encompassing the spectra of the OPG pump and downconverted signal as well as frequency upconversion to the visible (due to cascading of OPG and sum frequency generation [18]) at the output of the 2D nonlinear lattice.

The comparison between predicted (Fig. 4a-5a) and measured (Fig. 4c-5c) angle-averaged output spectra highlights the faithfulness of the broadband (2+1)D model in reproducing key features of the experiments, such as the relatively broad OPG signal emission in the 1-1.4 μm range and its double-peaked structure, due to the retracing behavior of the QPM curves for these working points, which are not too far from the zero group velocity dispersion point of the material ($\lambda_p = 860$ nm [18]). **A slight shift in the actual peak OPG wavelength is to be expected from uncertainties in Sellmeier equations [10, 11].** The comparison of OPG spectra allows also to identify a tail in the signal emission at longer wavelengths (1.4-1.6 μm), which consistently appeared in the experiments and yet not in the simulations. The observed signal output at these wave-

lengths might be then possibly due to other nonlinear effects not included in the $\chi^{(2)}$ model. The predictions of the broadband model appear quite accurate even when considering the outputs at shorter wavelengths, namely around the OPG pump and at visible wavelengths, where new spectral features arise as a result of quadratic cascading effects accompanying broadband TB-OPG. The 800nm-OPG pump experiences an asymmetric (predominantly blue shifted) sideband modulation upon propagation in the nonlinear lattice, appearing consistently in both experiments (Fig.4-5c, **where the broadening is still apparent, despite the use of a dichroic filter to suppress most of the pump throughput and the limited resolution (≈ 10 nm) used for spectral sampling**) and simulations (Fig. 4-5a). This is a signature of self-phase modulation induced by $\chi^{(2)}$ cascading [21], presumably acting here in combination with an asymmetric dispersion profile in the neighborhood of the current spectral workpoint, **and enhanced by a temporal walk-off between the pump and the down-converted signals**. The simulations provide also further insights on the nonlinear photonic crystal response in the 500-650 nm range, where several discrete emission peaks (at 502, 624, 573 and 602 nm for Fig.4, and 522, 573, 602 nm for Fig. 5) are observed in the experiments, matching well theoretical predictions. These signals in the visible are the result of cascaded sum-frequency generation (SFG) between the OPG pump and the multiple signal and idler beams it generates in the infrared (Fig. 2-3). A correct prediction of such SFG outputs relies critically on the accuracy in rendering the richness of the spectral and angular response of OPG in the infrared, hence is not possible with a standard CME QPM approach in these cases.

Conclusions. We introduced a model suitable for the analysis and the design of broadband multi-beam interactions stemming from the interplay of concurrent resonances in (2+1)D interaction geometries, typically arising in $\chi^{(2)}$ nonlinear photonic crystals. The model is particularly well suited for the treatment of multiple broadband parametric processes encompassing a broad spectrum of angular frequencies produced via concurrently noncollinear interactions. **Moreover, it could also be used to model ultrashort-pulse pumping regimes in tailored NPCs for more sophisticated engineering of the OPG output temporal profiles.** We analysed the specific case of twin-beam OPG in hexagonally poled LiTaO₃ crystals, where theoretical predictions could be compared with rich sets of experimental data. The study demonstrates the power of the method in capturing the complexity and richness of the interaction dynamics observed in the experiments, stemming from a coherent interplay of multiple OPG processes as well as cascaded effects in the 2D lattice. The proposed simulation tool provides rigorous quantitative estimations of conversion efficiencies and spectral and angular distributions, essential for device design and optimisation. Furthermore, its capabilities hold

promise for gaining deeper insights into the coherence properties of parametric downconversion in engineered nonlinear lattices, paving the way for the exploitation of the advanced functionalities affordable by $\chi^{(2)}$ nonlinear photonic crystals towards compact and efficient coherent sources for classical and quantum optics applications.

We gratefully acknowledge support to the research in Stockholm by the Carl Trygger foundation and the Swedish Research Council (VR-622-2010-526, VR-621-2011-4040 and ADOPT Linne Centre), in Brescia by MIUR (PRIN 2009P3K72Z, and PRIN 2012BFNWZ2) and in Lille by ANR (TOPWAVE).

References

1. S. Carrasco, A. V. Sergienko, B. E. A. Saleh, M. C. Teich, J. P. Torres, and L. Torner, Phys. Rev. A 73, 063802 (2006).
2. B. W. Mayer, C. R. Phillips, L. Gallmann, M. M. Fejer, and U. Keller, Opt. Lett. 38, 4265 (2013).
3. T. Topfer, K. P. Petrov, Y. Mine, D. Jundt, R. F. Curl, and F. K. Tittel, Appl. Opt. 36, 8042 (1997)
4. S. Witte and K. S. E. Eikema, IEEE J. Sel. Top. Quantum Electron. 18, 296 (2012).
5. N.G.R. Broderick, G.W. Ross, H.L. Offerhaus, D.J. Richardson and D.C. Hanna, Phys. Rev. Lett. 84, 4345 (2000).
6. V. Berger, Phys. Rev. Lett. 81, 4136 (1998)
7. K. Gallo, A. Pasquazi, S. Stivala, and G. Assanto, Phys. Rev. Lett. 100, 053901 (2008).
8. N. G. R. Broderick, R. T. Bratfalean, T. M. Monro, D. J. Richardson, and C. Martijn de Sterke, J. Opt. Soc. Am. B 19, 2263 (2002).
9. Y. Qin, C. Zhang, Y. Zhu, X. Hu, and G. Zhao, Phys. Rev. Lett. 100, 063902 (2008).
10. K. Gallo, M. Levenius, F. Laurell, and V. Pasiskevicius, Appl. Phys. Lett. 98, 161113 (2011)
11. M. Levenius, V. Pasiskevicius and K. Gallo, Appl. Phys. Lett. 101, 121114 (2012)
12. H.-C. Liu and A. H. Kung, Opt. Expr. 16, 9714 (2008).
13. M. Conforti, F. Baronio, and C. De Angelis, Phys. Rev. A 81, 053841 (2010).
14. M. Conforti, F. Baronio, and C. De Angelis, IEEE Photonics J. 2, 600 (2010).
15. M. Conforti, F. Baronio, C. De Angelis, M. Marangoni, and G. Cerullo, J. Opt. Soc. Am. B 28, 892 (2011).
16. M. Conforti, F. Baronio, and C. De Angelis, J. Opt. Soc. Am. B 28, 1231-1237 (2011).
17. M. Conforti and F. Baronio, J. Opt. Soc. Am. B 30, 1041 (2013).
18. M. Levenius, M. Conforti, F. Baronio, V. Pasiskevicius, F. Laurell, A. De Angelis, and K. Gallo, Opt. Lett. 37, 1727 (2012).
19. M. Kolesik, P. T. Whalen, and J. V. Moloney, J. Sel. Top. Quantum Electron. 18, 494 (2012).
20. F. Baronio, M. Conforti, C. De Angelis, A. Degasperis, M. Andreana, V. Couderc, and A. Barthelémy, Phys. Rev. Lett. 104, 113902 (2010).
21. R. DeSalvo, D. J. Hagan, M. Sheik-Bahae, G. Stegeman, E.W. Van Stryland, and H. Vanherzeele, Opt. Lett. 17, 28 (1992).

Informational Fifth Page

In this section, please provide full versions of citations to assist reviewers and editors (OL publishes a short form of citations) or any other information that would aid the peer-review process.

References

1. S. Carrasco, A. V. Sergienko, B. E. A. Saleh, M. C. Teich, J. P. Torres, and L. Torner, "Spectral engineering of entangled two-photon states", *Phys. Rev. A* **73**, 063802 (2006).
2. B. W. Mayer, C. R. Phillips, L. Gallmann, M. M. Fejer, and U. Keller, "Sub-four-cycle laser pulses directly from a high-repetition-rate optical parametric chirped-pulse amplifier at 3.4 μm ", *Opt. Lett.* **38**, 4265 (2013).
3. T. Topfer, K. P. Petrov, Y. Mine, D. Jundt, R. F. Curl, and F. K. Tittel, "Room-temperature mid-infrared laser sensor for trace gas detection", *Appl. Opt.* **36**, 8042 (1997)
4. S. Witte and K. S. E. Eikema, "Ultrafast Optical Parametric Chirped-Pulse Amplification", *IEEE J. Sel. Top. Quantum Electron.* **18**, 296 (2012).
5. N.G.R. Broderick, G.W. Ross, H.L. Offerhaus, D.J. Richardson and D.C. Hanna, "Hexagonally Poled Lithium Niobate: A Two-Dimensional Nonlinear Photonic Crystal" *Phys. Rev. Lett.* **84**, 4345 (2000).
6. V. Berger, , "Nonlinear Photonic Crystals" *Phys. Rev. Lett.* **81**, 4136 (1998)
7. K. Gallo , A. Pasquazi, S. Stivala, and G. Assanto, Parametric solitons in two-dimensional lattices of purely nonlinear origin, *Phys Rev Lett.* **100**, 053901 (2008).
8. N. G. R. Broderick, R. T. Bratfalean, T. M. Monro, D. J. Richardson, and C. Martijn de Sterke, "Temperature and wavelength tuning of second-, third-, and fourth-harmonic generation in a two-dimensional hexagonally poled nonlinear crystal," *J. Opt. Soc. Am. B* **19**, 2263 (2002).
9. Y. Qin, C. Zhang, Y. Zhu, X. Hu, and G. Zhao, *Phys. Rev. Lett.* **100**, 063902 (2008).
10. K. Gallo, M. Levenius, F. Laurell, and V. Pasiskevicius, "Twin-beam optical parametric generation in $\chi^{(2)}$ nonlinear photonic crystals" *Appl. Phys. Lett.* **98**, 161113 (2011)
11. M. Levenius, V. Pasiskevicius and K. Gallo, Angular degrees of freedom in twin-beam parametric downconversion, *Appl. Phys. Lett.* **101**, 121114 (2012)
12. H.-C. Liu and A. H. Kung, "Substantial gain enhancement for optical parametric amplification and oscillation in two-dimensional $\chi^{(2)}$ nonlinear photonic crystals", *Opt. Expr.* **16**, 9714 (2008).
13. M. Conforti, F. Baronio, and C. De Angelis, "Nonlinear envelope equation for broadband optical pulses in quadratic media," *Phys. Rev. A* **81**, 053841 (2010).
14. M. Conforti, F. Baronio, and C. De Angelis, "Ultra-broadband optical phenomena in quadratic nonlinear media," *IEEE Photonics J.* **2**, 600 (2010).
15. M. Conforti, F. Baronio, C. De Angelis, M. Marangoni, and G. Cerullo, "Theory and experiments on multistep parametric processes in nonlinear optics," *J. Opt. Soc. Am. B* **28**, 892 (2011).
16. M. Conforti, F. Baronio, and C. De Angelis, "Modeling of ultrabroadband and single-cycle phenomena in anisotropic quadratic crystals," *J. Opt. Soc. Am. B* **28**, 1231-1237 (2011).
17. M. Conforti and F. Baronio, "Extreme high-intensity and ultrabroadband interactions in anisotropic $\beta - \text{BaB}_2\text{O}_4$ crystals," *J. Opt. Soc. Am. B* **30**, 1041 (2013).
18. M. Levenius, M. Conforti, F. Baronio, V. Pasiskevicius, F. Laurell, A. De Angelis, and K. Gallo, Quadratic cascading effects in broadband optical parametric generation, *Opt. Lett.* **37**, 1727 (2012).
19. M. Kolesik, P. T. Whalen, and J. V. Moloney, "Theory and simulation of ultraintense pulse propagation in extended media," *J. Sel. Top. Quantum Electron.* **18**, 494 (2012).
20. F. Baronio, M. Conforti, C. De Angelis, A. Degasperis, M. Andreana, V. Couderc, and A. Barthelemy, "Velocity-Locked Solitary Waves in Quadratic Media", *Phys. Rev. Lett.* **104**, 113902 (2010).
21. R. DeSalvo, D. J. Hagan, M. Sheik-Bahae, G. Stegeman, E.W. Van Stryland, and H. Vanherzeele, "Self-focusing and self-defocusing by cascaded second-order effects in KTP", *Opt. Lett.* **17**, 28 (1992).